JBC Papers in Press. Published on October 15, 2020 as Manuscript RA120.014831
The latest version is at https://www.jbc.org/cgi/doi/10.1074/jbc.RA120.014831

Interrogation of kinase genetic interactions provides a global view of PAK1-mediated signal transduction pathways

Jae-Hong Kim[1], Yeojin Seo[1], Myungjin Jo[1,#a], Hyejin Jeon[1], Young-Seop Kim[1], Eun-Jung Kim[1], Donggun Seo[1], Won-Ha Lee[2], Sang Ryong Kim[2], Nozomu Yachie[3,#b], Quan Zhong[4], Marc Vidal[5], Frederick P. Roth[3], and Kyoungho Suk[1]*

[1] Department of Pharmacology, Brain Science and Engineering Institute, and Department of Biomedical Sciences, BK21 Plus KNU Biomedical Convergence Program, School of Medicine, Kyungpook National University, Daegu, 41944, Korea

[2] School of Life Sciences, Brain Korea 21 Plus KNU Creative BioResearch Group, Kyungpook National University, Daegu, 41566, Korea

[3] Donnelly Centre and Departments of Molecular Genetics and Computer Science, University of Toronto and Lunenfeld-Tanenbaum Research Institute, Sinai Health System, Toronto, Ontario M5G 1X5, Canada

[4] Department of Biological Sciences, Wright State University, Dayton, Ohio 45435, USA

[5] Center for Cancer Systems Biology (CCSB) and Department of Cancer Biology, Dana-Farber Cancer Institute, Boston, Massachusetts 02215, USA

[#a] Current address: Korea Brain Research Institute, Daegu, Korea

[#b] Current address: Synthetic Biology Division, Research Center for Advanced Science and Technology, The University of Tokyo, Tokyo, Japan; Institute for Advanced Bioscience, Keio University, Tsuruoka, Yamagata, Japan; PRESTO, Japan Science and Technology Agency (JST), Tokyo, 153-8904, Japan

*Corresponding author: Kyoungho Suk

E-mail: ksuk@knu.ac.kr

Running title: PAK1 genetic interaction in glioma cell behaviors

Keywords: kinase; glioma; genetic interaction; PAK1

Abstract

Kinases are critical components of intracellular signaling pathways and have been extensively investigated in regards to their roles in cancer. p21-activated kinase-1 (PAK1) is a serine/threonine kinase that has been previously implicated in numerous biological processes, such as cell migration, cell cycle progression, cell motility, invasion, and angiogenesis, in glioma and other cancers. However, the signaling network linked to PAK1 is not fully defined. We previously reported a large-scale yeast genetic interaction screen using toxicity as a readout to identify candidate PAK1 genetic interactions. *En masse* transformation of the PAK1 gene into 4,653 homozygous diploid S. cerevisiae yeast deletion mutants identified approximately 400 candidates that suppressed yeast toxicity. Here we selected 19 candidate PAK1 genetic interactions that had human orthologs and were expressed in glioma for further examination in mammalian cells, brain slice cultures, and orthotopic glioma models. RNAi and pharmacological inhibition of potential PAK1 interactors confirmed that *DPP4*, *KIF11*, *mTOR*, *PKM2*, *SGPP1*, *TTK*, and *YWHAE* regulate PAK1-induced cell migration, and revealed the importance of genes related to the mitotic spindle, proteolysis, autophagy, and metabolism in PAK1-mediated glioma cell migration, drug resistance, and proliferation. AKT1 was further identified as a downstream mediator of the PAK1-TTK genetic interaction. Taken together, these data provide a global view of PAK1-mediated signal transduction pathways and point to potential new drug targets for glioma therapy.

Introduction

Gliomas are tumors that occur in the brain and spinal cord. Glioma, which begins in the glial cells that surround neurons and help them function, is one of the most common types of malignant primary brain tumors. Treatment for glioma depends on the cell type, size, grade of malignancy, and location of the tumor. Treatment is usually a combination of surgery, radiation therapy, chemotherapy, and immunotherapy. Targeted drug therapy is preferred over conventional cytotoxic chemotherapy, as the targeted drug treatments focus on specific abnormalities present within cancer cells (1,2). By blocking these abnormalities, targeted drug treatments can cause cancer cells to die without affecting non-cancer cells (3). However, for the targeted drug therapy to be successfully developed and used in the clinic, one needs to better understand glioma cell behaviors (such as glioma cell migration/invasion, growth/proliferation, death/survival, and drug resistance) and related signaling pathways.

The signaling component “p21-activated kinase-1” (PAK1) is a serine/threonine kinase regulated by small GTP-binding proteins Cdc42 and Rac (4-7). This kinase affects a wide variety of cellular processes, such as cell motility, invasion, metastasis, growth, cell cycle progression, and angiogenesis. It has been previously implicated in a wide range of biological processes and the development of multiple types of cancer (8-14). More specifically, PAK1 has been previously implicated in cell death/survival, cell migration, and glioma (15-19). The expression level of PAK1 has been associated with the invasiveness of glioblastoma and survival time in patients with glioblastoma. Our own previous RNAi selection study indicated that the PAK kinase family regulates cell migration (20).

In this study, to better understand PAK1 kinase signaling pathways and to uncover new drug targets related to these pathways, we sought to

exploit the model eukaryote, which is amenable to rapid genome-scale experimentation to identify related functions. More specifically, we performed a genetic interaction screen for yeast deletions that can relieve the toxic effects of PAK1 expression in yeast, thereby identifying orthologous human genes as candidate genetic interaction partners. This is based on our previous study, in which overexpression of human PAK1 was toxic in yeast (21). Subsequent mammalian cell- and tissue-based validation experiments of these candidates identified multiple determinants of glioma cell migration, drug resistance, and proliferation, helping to elucidate the molecular mechanisms of PAK1-mediated carcinogenesis and other cellular behaviors.

Results

Identification of PAK1 genetic interactions

Functional analysis of kinase signaling pathways can be achieved by mapping genetic interaction networks for kinase genes (22-24). Here we sought genes for which perturbation modifies the activity of PAK1 kinase. Because *S. cerevisiae* has been a faithful model for many conserved aspects of eukaryotic cell biology (25), and because genetic interaction screens can be efficiently carried out in yeast, we used a pool of yeast deletion mutants that may modify the PAK1 toxicity phenotype. To identify PAK1 genetic interactions, we previously performed a genome-wide pooled screen to identify genetic interactions on the basis of toxicity modification (21). In that screen, PAK1 gene was first introduced into a pool of 4,653 homozygous diploid yeast deletion mutants such that each mutant harbors unique barcode sequences flanking the deletion locus (26). Second, PAK1 gene expression was induced by growth of yeast on galactose media. Third, yeast barcodes were amplified from deletion pool cultures. Finally, yeast barcode abundances were quantified using next-generation sequencing (Bar-seq) to identify fitness values of PAK1 genetic interactions (27). The relative abundance of each yeast barcode is a proxy for differential growth of the corresponding deletion strain, which allowed us to detect modulation of PAK1 toxicity in the absence of a specific yeast gene (28,29). For each of 4,653 yeast deletions, we identified the relative abundance of each deletion strain after selection in the presence of PAK1. Genetic interactions were identified on the basis of Z-scores: Z-score > 1.96 were identified as toxicity suppressors. Z-score 1.96 corresponds to confidence level 95% and p-value < 0.05, which is commonly used for statistically significance (30, 31). Among the 402 yeast suppressors of PAK1 toxicity, 131 yeast genes had human orthologs in our previous study (21). Human orthologs of the yeast toxicity suppressors were identified using the Karolinska Institute's InParanoid Database (http://inparanoid.sbc.su.se) (32). Out of these 131 genes, 19 genes (15%) that had human orthologs and were expressed in glioma cells were selected for further evaluation in the current study (Table 1 and Supplementary Figure 1).

Genetic interactions of PAK1 in mammalian cells

For functional evaluation of the PAK1 genetic interactions, siRNA-mediated knockdown in glioma cells was performed for these 20 orthologs of yeast interaction partners (note that, for yeast PYK2, we tested two orthologs, PKM1 and PKM2). Five siRNAs were designed for each PAK1 interaction partner (see Supplementary Table 1 for siRNA sequences; Supplementary Figure 1 for knockdown efficiency). In cases where all five siRNAs were ineffective in knocking down the expression of the corresponding gene, an additional siRNA was designed and synthesized. We tested

whether the expression knockdown of candidate genes could modify PAK1-induced cell migration and death/survival (see Supplementary Figure 2 for knockdown efficiency of siRNAs in PAK1 transfectants). Cell migration was first assessed using GL26 mouse glioma cells stably overexpressing PAK1 (Supplementary Figure 3). Because cells expressing either wild-type or a constitutively-active mutant *PAK1* cDNA showed similar PAK1 phosphorylation levels (Supplementary Figure 4) and enhanced cell migration phenotypes (Supplementary Figure 5), further experiments were performed only with wild-type PAK1-expressing GL26 cells (33). We cannot explain exactly whether exogenous PAK1 expression affected endogenous PAK1 activity. Overexpression of wild-type kinases often induces or enhances their own activity through auto-phosphorylation, etc. as a result of potential 'artifact' of overexpression (34-36). Thus, under the overexpression conditions, wild-type and constitutively-active mutant form of PAK1 might have exhibited similar levels of activation. We used two stable cell clones, GL26-PAK1-1 and GL26-PAK1-2, that each showed PAK1 overexpression and activation as indicated by phosphorylation. Overexpression of kinases is commonly used to determine the role of kinases in cancer-related signaling (34). Among the 5-6 siRNAs for each interaction partner, the one with the best knockdown efficiency was introduced into PAK1-transfected GL26 cells, and cell migration was assessed by wound healing assay. Among the 20 PAK1 interaction partners, knockdown of seven genes (*DPP4*, *KIF11*, *mTOR*, *PKM2*, *SGPP1*, *TTK*, and *YWHAE*) attenuated PAK1-induced cell migration, indicating that these genes related to proteases, mitotic spindle, autophagy, and metabolism of glucose and sphingolipids genetically interact with PAK1 to affect cell migration (Table 2 and Supplementary Figure 6). The cell migration assays were performed under the condition of no significant cytotoxicity (Supplementary Figure 7).

Pharmacological inhibitors were next used to further investigate the yeast-orthologous human genetic modifiers of PAK1 identified in the large-scale screen. Among the 20 PAK1 interaction partners tested by siRNA-mediated knockdown, pharmacological inhibitors were commercially available for six candidates. These six pharmacological inhibitors were used in wound healing assays in a manner similar to that used for the siRNA-mediated knockdown experiments. Among the six pharmacological inhibitors, four compounds (monastrol, KIF11 inhibitor; MPS1-IN-1, TTK inhibitor; rapamycin, mTOR inhibitor; vildagliptin, DPP4 inhibitor) reduced PAK1-induced GL26 glioma cell migration, while two compounds (fumagillin, METAP2 inhibitor; P-M2tide, PKM2 inhibitor) had no significant effects (Table 3 and Supplementary Figure 8). All inhibitors were used at optimal concentrations without apparent cytotoxicity based on the IC_{50} as reported in previous studies (37-40) and as determined by MTT cell viability assay (Supplementary Figure 9 and 10). The results of the pharmacological inhibitor experiments were consistent with those of the siRNA-mediated genetic knockdown experiments except for PKM2. PKM2 inhibitor P-M2tide did not significantly influence PAK1-induced cell migration, while siRNA-mediated knockdown of *PKM2* gene expression had significant effects. This discrepancy may be due to the complex role of PKM2 expression and activity in regulating cell behaviors (41-43).

For the functional evaluation of PAK1 genetic interactions with respect to cell death/survival phenotypes, glioma cells were used for anticancer drug toxicity testing and cell proliferation assays. PAK1-overexpressing GL26 glioma cells were transfected with siRNAs and then exposed to BCNU, an anticancer drug that is similar to temozolomide, which is commonly used in the treatment of glioma patients. Glioma cells stably expressing PAK1 clearly showed increased drug resistance

compared with that of parental cells. Knockdown of PAK1 interaction partner expression using siRNAs modulated glioma cell death (PAK1-induced drug resistance), as evaluated by LDH and MTT assays (Table 4 and Supplementary Figures 11 and 12), indicating genetic interactions between PAK1 and the knocked down genes (*DPP4*, *mTOR*, *SGPP1*, *TTK*, and *YWHAE*). A BCNU concentration of 200 μM was used for these experiments, based on dose-dependent toxicity test results (Supplementary Figure 13), and the mode of cell death was primarily apoptosis, as determined by caspase-3 activity assay (Supplementary Figure 14). Differences between controls and PAK1-overexpressing cells were modest in some of the results. However, the difference was statistically significant in the key comparisons.

Functional evaluation of PAK1 genetic interactions with respect to glioma cell proliferation was performed using the six pharmacological inhibitors of the interaction partners. The proliferation rate of PAK1-expressing GL26 glioma cells was measured by real-time imaging of cell confluence using IncuCyte (44), and the results are presented as the cell doubling time. Inhibition of DPP4, METAP2, mTOR, PKM2, and TTK attenuated PAK1-induced effects on glioma cell proliferation, indicating genetic interactions between PAK1 and these five genes in terms of cell proliferation (Table 5 and Supplementary Figure 15). Taken together, these results indicate that PAK1 exhibited similar genetic interactions with respect to cell migration, cell death/survival, and proliferation phenotypes in the cultured glioma cell model. These results suggest that the PAK1 genetic interactions identified in the yeast-based screen may be relevant to glioma growth, invasion, and chemoresistance *in vivo* (see below).

We next tested the impact of the candidate modifiers on the expression of the *PAK1* gene. For none of the eight major interaction partners did siRNA-mediated knockdown significantly affect the expression levels of *PAK1* in glioma cells (Supplementary Figure 16), indicating that the modulation of PAK1-mediated effects on cell phenotypes (cell migration, cell death/survival, and proliferation) by the genetic interactors was not due to the downregulation of *PAK1* gene expression.

Evaluation of genetic interactions of PAK1 in brain slice cultures and orthotopic glioma models

Among the 20 genetic interactors of PAK1 tested in mammalian cells, DPP4, KIF11, METAP2, mTOR, and TTK were subjected to subsequent evaluation using brain slice cultures (Figure 1). In this experiment, the invasive capacity of glioma cells transplanted onto organotypic cultures of brain slices was evaluated. To examine the genetic interactions between PAK1 and its interacting partners, GL26 glioma cells overexpressing PAK1 were transplanted onto brain slices, and the degree of glioma cell invasion was monitored in the presence of specific inhibitors of the five interacting partners. Compared with empty vector-transfected control cells, PAK1-transfected glioma cells (GL26-PAK1-1, GL26-PAK1-2) showed higher degrees of cell invasion when transplanted onto brain slice cultures. The PAK1-induced enhancement of glioma cell invasion was diminished by MPS1-IN-1 (TTK inhibitor), rapamycin (mTOR inhibitor), and vildagliptin (DPP4 inhibitor) but not by fumagillin (METAP2 inhibitor) or monastrol (KIF11 inhibitor) (Figure 1). The discrepancy between these results and the wound healing assay performed in a cultured cell line (Table 3) may reflect differences in the migration and invasion capacity of glioma cells in the distinct microenvironments of the two assay systems.

Nevertheless, PAK1 genetic interactions with DPP4, mTOR, and TTK were consistent in both assays.

Next, an orthotopic mouse model of glioma was used to test the genetic interactions between PAK1 and DPP4, mTOR, and TTK. These interaction partners were selected for genetic interaction evaluation *in vivo* based on the brain slice culture experiments. PAK1-expressing GL26 glioma cells (GL26-PAK1-1) were injected into the striatum of the mouse brain, and glioma behaviors were assessed by bioluminescence live imaging and histological analyses. Glioma growth was continuously measured up to 16 days after intracranial implantation of glioma cells using real-time bioluminescence imaging to detect GL26 glioma cells transfected with both PAK1 and luciferase. Pharmacological inhibition of the interaction partners by specific inhibitors reduced PAK1-induced increases in glioma growth (Figure 2), volume, and invasion in the mouse brain (Figure 3 and Supplementary Figures 17 and 18). At the end of the live imaging analysis, animals were sacrificed for histological analyses. Glioma volume was measured by quantitative digital image analysis of serial brain sections containing tumors (Figure 3*A*, *B*). Glioma invasion was quantified by particle analysis of threshold images (Figure 3*C* and Supplementary Figure 17) or invasive finger analysis (Supplementary Figure 18) of tumor-bearing brain sections. The results indicated strong genetic interactions between PAK1 and these partners (DPP4, mTOR, and TTK) with respect to glioma growth and invasion *in vivo*.

AKT1 as a common downstream mediator of the PAK1-TTK genetic interaction

Among the genetic interactions confirmed in brain slice cultures and orthotopic glioma models, a subsequent mechanistic study focused on the genetic interaction between PAK1 and TTK. Because AKT1 has been previously implicated in cell migration and is known to act downstream of the PAK1 signaling pathway (45-49), the potential role of AKT1 in the genetic interaction between PAK1 and TTK was investigated. AKT1 was identified as a common downstream component of PAK1- and TTK-mediated cell migration signaling pathways (Figure 4). Transient overexpression of either PAK1 or TTK induced AKT1 phosphorylation in NIH3T3 cells (Figure 4*B*). Inhibition of TTK using MPS1-IN-1 reduced PAK1-induced AKT1 phosphorylation; however, PAK1 inhibition using IPA3 did not significantly affect TTK-induced AKT1 phosphorylation (Figure 4*B*). Similarly, TTK inhibition decreased PAK1-mediated cell migration, while PAK1 inhibition did not significantly influence TTK-mediated cell migration (Figure 4*C*), indicating that PAK1 acts upstream of TTK in the cell migration signaling pathway (Figure 4*D*). Pharmacological inhibitors were used at concentrations that did not exert cytotoxic effects (Supplementary Figure 19). Moreover, PAK1 overexpression increased TTK expression at both the mRNA and protein levels (Supplementary Figure 20), further suggesting that PAK1 acts upstream of TTK. Taken together, these results suggest that the genetic interaction between PAK1 and TTK mediating multiple behaviors of glioma cells may involve: i) activation of the common downstream mediator AKT1; and ii) PAK1 upregulation of TTK expression. The molecular mechanisms of the genetic interactions between PAK1 and DPP4 or mTOR, which were confirmed in the *in vivo* glioma model, need to be further investigated; however, at least the PAK1-mTOR genetic interaction could be explained by a pathway similar to that of the PAK1-TTK interaction (Figure 4*D*), as mTOR has been previously shown to activate AKT1 (50,51).

Validation of the genetic interactions via overexpression of PAK1 interactors

To further demonstrate the genetic interactions between PAK1 and its interactors, we tested whether the overexpression of some of the PAK1 genetic interactors rescues cell migration, proliferation, drug resistance, and glioma invasion under PAK1-inhibited condition. For this, mTOR, PKM2, TTK, and AKT1 were either activated or overexpressed in GL26 glioma cells, which were treated with a PAK1 inhibitor (IPA3). Rheb cDNA overexpression was used to activate mTOR pathway (52), DASA-58 was used as a PKM2 activator, TTK cDNA was overexpressed, SC-79 was used as an AKT1 activator, or Myr-AKT1 cDNA (53) was overexpressed. All compounds were used at the concentrations of no significant cytotoxicity (Supplementary Figure 21), and the overexpression of the PAK1 interactors was confirmed by western blot or fluorescence imaging (Supplementary Figure 22). In the subsequent experiments, migration (Supplementary Figures 23-25), proliferation (Supplementary Figure 26), drug resistance (Supplementary Figure 27), and glioma invasion (Supplementary Figure 28) were all rescued by either activation or overexpression of mTOR, PKM2, TTK, or AKT1 in PAK1-inhibited glioma cells, further supporting the genetic interactions between PAK1 and its effector molecules.

Discussion

Analyses of PAK1 genetic interactions identified many new potential determinants of glioma cell migration, drug resistance, and growth. Among the 131 human genetic interaction partners of PAK1, many were previously associated with cell motility and death/survival. Interestingly, PAK1 is also known to be involved in glioma cell migration, death/survival, and proliferation (15-19). Therefore, several interaction partners of PAK1 were chosen for further investigation using cultured glioma cells, organotypic brain slice cultures, and an orthotopic *in vivo* glioma model. Genetic interactions between PAK1 and the candidate genes were evaluated in these experimental models with respect to various glioma cell behaviors, such as cell migration, invasion, drug resistance, growth, and proliferation. During this process, a few candidates (DPP4, mTOR, and TTK) were selected for further evaluation of their consistent genetic interactions with PAK1 in an animal model. Finally, one of the genetic interaction partners, TTK, which is itself a protein kinase and has been previously implicated in mitotic spindle regulation (54,55), was subjected to mechanistic study. After demonstrating the important role of TTK in PAK1-induced glioma cell migration, drug resistance, and growth *in vitro* and *in vivo*, we further found that AKT1 is a point of convergence in the signaling pathways of the two kinases PAK1 and TTK.

Overexpression of either PAK1 or TTK induced AKT1 activation and enhanced cell migration. PAK1 was found to be upstream of TTK in the cell migration pathway on the basis of signaling pathway analyses using kinase inhibitors and transient overexpression of the kinases (Figure 4). However, no protein-protein interaction between PAK1 and TTK was observed in the co-immunoprecipitation assay (Supplementary Figure 29). PAK1 and TTK seem to share a common signaling pathway that leads to AKT1 activation and cell migration (Figure 4*D*). This relationship among the three kinases (PAK1, TTK, and AKT1) may be important in view of glioma chemotherapy. Inhibition of the common AKT1 pathway may have therapeutic potential for either PAK1- or TTK-mediated oncogenic events. Our results also provide a mechanistic basis for mono- or combination chemotherapy of malignant glioma in the future.

In the evaluation of PAK1 genetic interactions using mammalian cells, we only tested 20 genetic interaction partners among the 131 candidates. The other 111 interaction partners with human orthologs may also be relevant in the context of PAK1 and glioma. In fact, the 131 candidates were associated with many molecular functions and biological processes (Supplementary Table 2 and 3), which can be further explored to better understand glioma pathogenesis. However, it remains to be determined to what extent genetic interaction discovered in yeast based on the fitness/toxicity of PAK1 would be relevant in human glioma. Among the 20 PAK1 genetic interactions, not all leads from the yeast toxicity screen were relevant in mammalian cell phenotypes, such as mouse glioma cell migration, drug resistance, and growth. This might be due to differences in the mechanisms underlying the modification of yeast toxicity and mammalian cell phenotypes. For example, the mechanism of PAK1 toxicity suppression by deletion of DAP2, KIP1, MAP2, TOR1, or SAT4 in yeast may be different from that of modification of glioma cell phenotypes by knockdown of their orthologs (DPP4, KIF11, METAP2, mTOR, or TTK) in mammalian cells (see Table 1 for the list of PAK1 genetic interactions in yeast and their human orthologs). Despite these limitations, current results provided testable and subsequently validated hypotheses relating to biological functions of PAK1 in glioma. Moreover, our analyses newly identified numerous determinants of glioma cell migration, drug resistance, and growth as potential drug targets for glioma treatment.

Materials and Methods

Yeast strains, media, and plasmids

BY4742 (Mat α; *his3Δ1*; *leu2Δ0*, *lys2Δ0*; *ura3Δ0*) was used as a wild-type yeast strain in this study. The Homozygous Diploid Complete Set of Yeast Deletion Clones and Homozygous Diploid Yeast Deletion Pools were purchased from Invitrogen (Carlsbad, CA, USA). Yeast cells were grown in rich medium (YPD) or synthetic medium lacking leucine and containing 2% glucose (SD-Leu), raffinose (SRaf-Leu), or galactose (SGal-Leu). Wild-type and constitutively active mutant (T423E) *PAK1* cDNAs were kindly provided by Prof. Eung-Gook Kim at Chungbuk National University (Cheongju, Republic of Korea) (56-58). The Gateway LR reaction was used to shuttle PAK1 cDNA into pAG425GAL-ccdB (Addgene, Cambridge, MA, USA) (59) for yeast expression. All plasmids were 2-μm-based and under the control of the *GAL1* promoter. All constructs were verified by Sanger sequencing. PAK1 cDNA in pAG425GAL (yeast destination vector) were transformed into BY4742 or homozygous diploid deletion strains. All yeast strains were grown at 30°C according to the standard protocol. We used the LiAc/SS carrier DNA/PEG method to transform yeast with plasmid DNA as previously described (60). For functional studies in mammalian cells or mice, the Gateway LR reaction was used to shuttle PAK1 cDNA into pDS-GFP-XB (Invitrogen) destination vectors.

PAK1 genetic interaction screen

The screen for genetic modifiers of PAK1 in *S. cerevisiae* was carried out as described (Supplementary Figure 30) (21). Briefly, PAK1 cDNAs were transformed into homozygous diploid yeast deletion pools containing 4,653 individual deletion clones. Transformants were incubated in SD-Leu medium for 16 hr. The cells were washed twice with PBS and then incubated in SGal-Leu medium for 2 days. Cells remaining in glucose-containing SD-Leu medium were used as a control. Genomic DNA

was isolated from cells harvested after pooled growth. Each 20-mer UPTAG barcode was amplified and sequenced using a Genome Analyzer (Illumina, San Diego, CA, USA) according to the manufacturer's protocols.

Cell cultures and reagents

NIH3T3 mouse fibroblasts were purchased from ATCC, and GL26 mouse glioma cells were kindly provided by Prof. Eun Jung Park (Cancer Immunology Branch, National Cancer Center, Goyang, Gyeonggi, Republic of Korea). Both cell lines were authenticated, tested negative for *Mycoplasma*, and maintained in Dulbecco's modified Eagle's medium (DMEM) supplemented with 10% heat-inactivated fetal bovine serum (FBS) and 100 U/ml penicillin at 37°C. For the stable transfection of GL26 cells, cells were transfected with pDS-GFP-XB containing wild-type or mutant (T423E) human *PAK1* cDNA using Fugene HD transfection reagent (Invitrogen), according to the manufacturer's instructions. Stable transfectants were established in the presence of 1 mg/ml G418 (Sigma-Aldrich, St. Louis, MO, USA), and their GFP expression was observed under fluorescence microscopy (BX50; Olympus, Tokyo, Japan). Desalted and preannealed siRNA duplexes were purchased from Genolution Pharmaceuticals (Seoul, Korea). The siRNAs were designed using a proprietary algorithm devised by Genolution Pharmaceuticals. The siRNAs were transfected into cells using RNAi MAX reagent (Invitrogen). Transient transfection of NIH3T3 and GL26 cells with human *PAK1*, *TTK*, or *AKT* cDNA was similarly performed using Fugene HD or Lipofectamine 2000 transfection reagent (Thermo Fisher Scientific, Waltham, MA, USA). Rapamycin (Cat No. 553210) was purchased from Calbiochem (San Diego, CA, USA). Monastrol (Cat No. M8515) was purchased from Sigma-Aldrich. MPS1-IN-1 (Cat No. 5142) and IPA3 (Cat No. 3622) were purchased from Tocris Bioscience (Bristol, UK). Fumagillin (Cat No. ab141527) was purchased from Abcam (Cambridge, MA, USA). P-M2tide (Cat No. BML-P239) was purchased from Enzo Life Sciences (Farmingdale, NY, USA). Vildagliptin (Cat No. S3033) and DASA-58 (Cat No. S7928) were purchased from Selleckchem (Houston, TX, USA). SC-79 (Cat No. 4635) was purchased from Tocris Bioscience (Bristol, UK). Summary of pharmacological agents used in this study is shown in Supplementary Table 4.

Reverse transcription polymerase chain reaction (RT-PCR)

Isolated cells were homogenized using TRIzol reagent (Invitrogen) to obtain total RNA. cDNA was then synthesized using Superscript II (Invitrogen) and oligo(dT) primer. Traditional PCR amplification was conducted using specific primer sets (Supplementary Table 5). Electrophoresis was conducted to analyze PCR reactions using 1.2% agarose gels.

Wound healing assay

In vitro wound healing assay was performed using the IncuCyte ZOOM Live-Cell Imaging system (Essen Bioscience, Ann Arbor, MI, USA). Cells were seeded at a density of 2.5×10^4 cells/well in IncuCyte® ImageLock plates. Cells were then treated with mitomycin C (5 μg/ml) for 2 hr before introduction of a wound to inhibit cell proliferation. Wounds were made with an IncuCyte WoundMaker™, and plates were automatically analyzed for wound closure with the IncuCyte ZOOM Live-Cell Imaging system. siRNA transfection was performed 48 hr before wound introduction. Alternatively, inhibitor treatment was performed immediately after wound introduction. Real-time images were acquired every 2–3 hr for 48 hr. Cell

confluence was quantified using time-lapse curves generated by IncuCyte ZOOM software and converted to wound closure velocity (μm^2/hr).

Manual scratch wound healing assays were performed as previously described (61). In brief, scratch wounds were created using a 10-µl pipette tip on confluent cell monolayers in 24-well culture plates containing DMEM with 10% FBS and 100 U/ml penicillin. Cells were incubated at 37°C under 5% CO_2 during migration of the monolayer into the cleared wound area. The wound area was observed by microscopy (×100 magnification). Relative cell migration distance was determined by measuring the wound width and subtracting this from the initial value: Cell migration distance = Initial wound width at day 0 – Wound width on the day of measurement. Three non-overlapping fields were selected and examined in each well (three wells per experimental group). The results are presented as the fold increase in migration distance (wound closure).

Boyden chamber migration assay

Cell migration was also determined using a 48-well Boyden chamber (Neuroprobe, Gaithersburg, MD, USA), according to the manufacturer's instructions. DMEM with 10% FBS was placed into the base wells and separated from the top wells by polycarbonate filters (8-µm pore size; 25 × 80 mm, polyvinylpyrrolidone-free; Neuroprobe). Cells were harvested by trypsinization, washed once with serum-free DMEM containing 0.5 mg/ml soybean trypsin inhibitor (Sigma-Aldrich), and washed twice with serum-free DMEM. Cells were resuspended in serum-free medium and added to the upper chamber at 8×10^3 cells/well. Cells were incubated for 16 hr at 37°C under 5% CO_2. At the end of the experiment, cells were fixed with methanol for 10 min and stained with Mayer's hematoxylin (Dakocytomation, Glostrup, Denmark) for 20 min. Cells on the upper slide of the membrane were then removed using a cotton swab. Photomicrographs of five randomly chosen fields were taken (×100 magnification), and cells were enumerated to calculate the average number of cells that had migrated.

Cell viability assays

For 3-[4,5-dimethylthiazol-2-yl]-2,5-diphenyltetrazolium bromide (MTT) assay, cells were treated with various reagents for the designated time period. After treatment, MTT (0.5 mg/ml; Sigma-Aldrich) was added to the cells and incubated at 37°C in a 5% CO_2 incubator. After 2 hr, DMSO was added to dissolve the insoluble crystals, and absorbance was measured using a microplate reader (Anthos Labtec Instruments, Wals, Austria) at 570 nm. For lactate dehydrogenase (LDH) assay, cells were seeded at a density of 2×10^4 cells/well in 96-well plates. Cells were transfected with siRNAs and treated with bis-chloroethylnitrosourea (BCNU) at 48 hr after cell transfection. After 24 hr, culture media were transferred to a new 96-well plate, and LDH activity was measured using the Promega Cytotoxicity kit (Madison, WI, USA) according to the manufacturer's instructions. LDH activity is presented as the percentage of LDH in the culture medium following BCNU or vehicle treatment relative to the maximum LDH release following treatment with cell lysis solution.

Measurement of caspase-3 activity

Caspase-3 activities were assessed using a caspase-3 colorimetric assay kit (Abcam) according to the manufacturer's protocol. Briefly, cells were collected and resuspended in

lysis buffer containing 50 mM HEPES (pH 7.4), 0.1% CAHPS, 1 mM DTT, 0.1 mM EDTA, and 0.1% Triton X-100. Following incubation for 30 min on ice, cell lysate was centrifuged at 11,000 ×*g* for 10 min at 4°C, and the protein concentration in the supernatant was measured using the Bradford dye method. The supernatants were incubated with reaction buffer containing 2 mM Ac-DEVD-AFC and 10 mM DTT at 37°C for 2 hr. Caspase-3 activity was determined by measuring the absorbance at 405 nm.

Cell proliferation assay

The IncuCyte ZOOM Live-Cell Imaging system (Essen Bioscience) was used for monitoring cell proliferation. Cells were seeded at a density of 1 × 10^3 cells/well in IncuCyte® ImageLock plates. After 24 hr, cells were treated with various compounds and analyzed with the IncuCyte ZOOM Live-Cell Imaging system. Real-time images of cell confluence were acquired every 2–3 hr for 72 hr. Cell proliferation was quantified based on time-lapse curves generated by IncuCyte ZOOM software and is presented as cell doubling time.

Western blotting analysis

Cultured cells were lysed in triple-detergent lysis buffer (50 mM Tris-HCl [pH 8], 150 mM NaCl, 0.02% sodium azide, 0.1% $NaDodSO_4$ [SDS], 1% Nonidet P-40, 0.5% sodium deoxycholate, and 1 mM PMSF). Protein concentrations in cell lysates were determined using a protein assay kit (Bio-Rad, Hercules, CA, USA). Each protein sample was separated by 8% or 12% SDS-PAGE, blotted, and incubated overnight at 4°C using the following primary antibodies: anti-PAK1 (Cell Signaling Technology, Danvers, MA, USA, #2602), anti-phospho-PAK1/2 (Ser144/Ser141, Cell Signaling Technology, #2606), anti-TTK (Origene, Rockville, MD, USA, TA314651), anti-phospho-AKT (Ser473, Cell Signaling Technology, #9271), anti-AKT (Cell Signaling Technology, #9272), anti-p-p70S6K (Thr389, Cell Signaling, #9234), anti-p70S6K (Cell Signaling, #2708), anti-GFP (Santa Cruz Biotechnology, Dallas, TX, USA, sc-9996), anti-Flag (Sigma Aldrich, F7425), anti-α-tubulin (Sigma-Aldrich, T5168), and anti-β-actin (Thermo Fisher Scientific, MAS-15739). Afterwards, samples were incubated with HRP-conjugated secondary antibodies and detected using ECL solution.

Mice and animal care procedures

Female C57BL/6 mice (8 weeks old) were obtained from Samtaco (Osan, South Korea). All animal experiments were performed in accordance with animal protocols and guidelines approved by the Animal Care Committee at Kyungpook National University (No. KNU 2018-0084).

Generation of GL26 glioma spheroids

GL25 glioma cell suspensions (GL26-Empty, GL26-PAK1-1, and GL26-PAK1-2) were dispensed into ULA 96-well round-bottomed plates (Corning Inc., Corning, NY, USA) using a multichannel pipette at optimized densities (5 × 10^4 cells/well). Plates were incubated for 4 days at 37°C, 5% CO_2, and 95% humidity for spheroid formation.

Glioma invasion assay in organotypic brain slice cultures

Organotypic brain slice cultures were prepared by the interface method and grown for the first three days in serum-based culture medium as previously described (62-66). Glioma spheroids (200–400 μm) were labeled with 25 μg/ml 1,1′-dioctadecyl-3,3,3′,3′ tetramethylindocarbocyanine perchlorate (DiI) solution (Molecular Probes, Invitrogen) for 24 hr, washed, and implanted onto brain slice cultures in the area between the cortex and striatum close to the corpus callosum. To enable capture and correct placement onto brain slice cultures, only spheroids of 200–400 μm were used. Glioma cell invasion was visualized using confocal microscopy (Nikon ECLIPSE TE2000-E inverted microscope). Confocal z-stacks with 20-μm steps were recorded and superimposed into a single image representing the entire spheroid. This procedure was repeated on day 2 and day 6. In the superimposed images, the area of each spheroid was measured using the software Visiomorph (Visiopharm, Hørsholm, Denmark). The spheroids were outlined at the spheroid border, identifying the beginning of the invasion zone. The area of the invasive cells was also measured using a classifier identifying the area of DiI staining, representing only the invasive cells and not the spheroids.

Surgery for mouse orthotopic model of glioma

Glioma cell transplantation surgery was performed as described previously (67,68) with minor modifications. Mice were anesthetized initially using 2–4% isoflurane and placed on a mini-vent (Harvard Apparatus, Cambridge, MA, USA). Anesthesia was maintained at 1.5% throughout the surgery. To visualize the transplanted glioma cells, GL26 cells were infected with retroviruses carrying the enhanced firefly luciferase gene (*effLuc*) and a Thy1.1 (CD90.1) marker. The infected cells were isolated by magnetic-activated cell sorting (MACS; Miltenyi Biotech Ltd., Bisley, Surrey, UK) using monoclonal anti-CD90.1 Ab conjugated to magnetic microbeads. The effLuc-expressing GL26 cells were stably transfected with either empty vector or PAK1 constructs to generate GL26-empty/effLuc or GL26-PAK1-1/effLuc cells, respectively. These cells were delivered into the right striatum using a 25-gauge (G) Hamilton syringe and stereotactic frame (Kopf, Tujunga, CA, USA) at an injection rate of 1 μl/min (9×10^5 cells in 2.5 μl of PBS). After tumor implantation, mice received an intratumoral injection of inhibitors (MPS1-IN-1, rapamycin, and vildagliptin) using a 26-G Hamilton syringe attached to an automated microinjector. Infusion proceeded at a rate of 0.5 μl/min for 10 min. At the end of the injection, the needle was left in place for an additional 10 min before being retracted slowly.

Bioluminescence imaging of intracranial glioma growth

Intracranial tumor growth was assessed by bioluminescence imaging using the Xenogen IVIS 200 small-animal imaging system (Xenogen Corp., Alameda, CA, USA). The IVIS 200 cooled CCD camera system was used for emitted light acquisition and Living Image software (Xenogen Corp.) was used for data analysis as an overlay on IGOR software (Wavemetrics Corporation, Lake Oswego, OR, USA). Animals received a 200-μl intraperitoneal injection of D-luciferin (Xenogen Corp.) at a concentration of 15 mg/ml under 1–2% inhaled isoflurane anesthesia. Identical illumination settings (lamp voltage, filters, f/stop, field of views, binning, excitation filter block, and emission filter open) were used for acquiring all images. Data were analyzed using total photon flux emission (photons/s) in an ROI covering the entire brain. After euthanasia with pentobarbital (100 mg/kg, ip) followed by extensive perfusion with 4% paraformaldehyde, brains were removed,

incubated in 30% sucrose (w/v in PBS) for 18 hr, and frozen over liquid nitrogen.

Analysis of tumor volume and invasion in the mouse model of glioma

For serial sectioning and visualization of tumors, fixed mouse brains were processed routinely, embedded in optimal cutting temperature (OCT) compound for cryosectioning, and serially sectioned at 9-µm. Coronal sections were stained with Mayer's modified hematoxylin (100%, 2 min). Serial sections at 150-µm intervals were used for tumor volume and invasion measurements.

For analysis of tumor volume, sections containing tumor were used for quantitative digital image analysis (69). Each section was imaged in its entirety using an Axiovert 35 light microscope (Zeiss, Chester, VA, USA) equipped with a digital camera (Sensys, Roper Scientific, Trenton, NJ, USA) and RGB filter (Microcolor GmbH, Straufhein, Germany). Areas occupied by tumor were outlined in a blinded fashion using a pre-selected cutoff, and images were acquired and digitized via Metamorph (Universal Imaging Corp., Westchester, PA, USA). The sum of all tumor areas was recorded (69).

For analysis of tumor invasion, the tumor-bearing hemisphere was recorded in a series of 50× magnification images using Spot Advanced software (Diagnostic Instruments, Sterling Heights, MI, USA). Photomerge automation for Photoshop CS4 (Adobe, San Jose, CA, USA) was then used to reconstruct the entire series into a single image. Inversion of the image into a black-on-white image was used to isolate the tumor, and the threshold was adjusted to distinguish the tumor from any nonspecific background staining. Finally, the ImageJ Analyze Particles (National Institutes of Health, Bethesda, MD, USA) function was used to quantify the total number of discrete particles. Alternatively, tumor invasion was quantified based on the number of invasive fingers, as described previously (70-72). Finger-like tumor projections into the adjacent normal brain tissue at the interface between the tumor and normal tissue were counted in images at ×20 magnification to assess tumor invasion in this area.

Statistical analysis

All data are presented as the mean ± s.d. from three or more independent experiments, unless otherwise stated. Different treatments were compared with Student's *t*-test or one-way ANOVA with Dunnett's multiple comparisons test using SPSS software (version 18.0; SPSS Inc., Chicago, IL, USA). Differences with a *P*-value of less than 0.05 were considered statistically significant. The sample size for experiments was chosen to ensure adequate statistical power on the basis of G*power 3.1 software (73).

Data Availability Statement

All data pertinent to this work are contained within this manuscript or available upon request. For requests, please contact: Kyoungho Suk, Kyungpook National University, ksuk@knu.ac.kr.

Funding and additional information

This work was supported by a National Research Foundation of Korea (NRF) grant funded by the Korea government (MSIP) (2018R1A2A1A05077118). F.P.R. was supported by US National Institutes of Health (NIH) grants HG001715 and HG004233, by the Canada Excellence Research Chairs Program, and by the Krembil and Avon Foundations. N.Y. was supported by a JSPS fellowship (Research Abroad), Japan Society for the Promotion of Science, a Banting Postdoctoral Fellowship, National Sciences and Engineering Research Council of Canada, and PRESTO research grant by Japan Science and Technology Agency (JST).

Conflict of Interest: The authors declare no conflicts of interest in regards to this manuscript.

References

1. Le Rhun, E., Preusser, M., Roth, P., Reardon, D. A., van den Bent, M., Wen, P., Reifenberger, G., and Weller, M. (2019) Molecular targeted therapy of glioblastoma. *Cancer Treat Rev* **80**, 101896
2. Miller, J. J., and Wen, P. Y. (2016) Emerging targeted therapies for glioma. *Expert Opin Emerg Drugs* **21**, 441-452
3. Mooney, J., Bernstock, J. D., Ilyas, A., Ibrahim, A., Yamashita, D., Markert, J. M., and Nakano, I. (2019) Current Approaches and Challenges in the Molecular Therapeutic Targeting of Glioblastoma. *World Neurosurg* **129**, 90-100
4. Zhao, Z. S., and Manser, E. (2012) PAK family kinases: Physiological roles and regulation. *Cell Logist.* **2**, 59-68
5. Teramoto, H., Crespo, P., Coso, O. A., Igishi, T., Xu, N., and Gutkind, J. S. (1996) The small GTP-binding protein rho activates c-Jun N-terminal kinases/stress-activated protein kinases in human kidney 293T cells. Evidence for a Pak-independent signaling pathway. *J. Biol. Chem.* **271**, 25731-25734
6. Ong, C. C., Jubb, A. M., Zhou, W., Haverty, P. M., Harris, A. L., Belvin, M., Friedman, L. S., Koeppen, H., and Hoeflich, K. P. (2011) p21-activated kinase 1: PAK'ed with potential. *Oncotarget* **2**, 491-496
7. Taglieri, D. M., Ushio-Fukai, M., and Monasky, M. M. (2014) P21-activated kinase in inflammatory and cardiovascular disease. *Cell Signal.* **26**, 2060-2069
8. van Zijl, F., Krupitza, G., and Mikulits, W. (2011) Initial steps of metastasis: cell invasion and endothelial transmigration. *Mutat. Res.* **728**, 23-34
9. Gupta, S. C., Kim, J. H., Prasad, S., and Aggarwal, B. B. (2010) Regulation of survival, proliferation, invasion, angiogenesis, and metastasis of tumor cells through modulation of inflammatory pathways by nutraceuticals. *Cancer Metastasis Rev.* **29**, 405-434

10. Kichina, J. V., Goc, A., Al-Husein, B., Somanath, P. R., and Kandel, E. S. (2010) PAK1 as a therapeutic target. *Expert Opin. Ther. Targets* **14**, 703-725
11. Bright, M. D., Garner, A. P., and Ridley, A. J. (2009) PAK1 and PAK2 have different roles in HGF-induced morphological responses. *Cell Signal.* **21**, 1738-1747
12. Coniglio, S. J., Zavarella, S., and Symons, M. H. (2008) Pak1 and Pak2 mediate tumor cell invasion through distinct signaling mechanisms. *Mol. Cell Biol.* **28**, 4162-4172
13. Rane, C. K., and Minden, A. (2018) P21 activated kinase signaling in cancer. *Semin. Cancer Biol.*
14. Semenova, G., and Chernoff, J. (2017) Targeting PAK1. *Biochem. Soc. Trans.* **45**, 79-88
15. Parvathy, M., Sreeja, S., Kumar, R., and Pillai, M. R. (2016) Potential role of p21 Activated Kinase 1 (PAK1) in the invasion and motility of oral cancer cells. *BMC Cancer* **16 Suppl 1**, 293
16. Wang, G., Zhang, Q., Song, Y., Wang, X., Guo, Q., Zhang, J., Li, J., Han, Y., Miao, Z., and Li, F. (2015) PAK1 regulates RUFY3-mediated gastric cancer cell migration and invasion. *Cell Death Dis.* **6**, e1682
17. Ong, C. C., Jubb, A. M., Haverty, P. M., Zhou, W., Tran, V., Truong, T., Turley, H., O'Brien, T., Vucic, D., Harris, A. L., Belvin, M., Friedman, L. S., Blackwood, E. M., Koeppen, H., and Hoeflich, K. P. (2011) Targeting p21-activated kinase 1 (PAK1) to induce apoptosis of tumor cells. *Proc. Natl. Acad. Sci. U. S. A.* **108**, 7177-7182
18. Yuan, Z. Q., Kim, D., Kaneko, S., Sussman, M., Bokoch, G. M., Kruh, G. D., Nicosia, S. V., Testa, J. R., and Cheng, J. Q. (2005) ArgBP2gamma interacts with Akt and p21-activated kinase-1 and promotes cell survival. *J. Biol. Chem.* **280**, 21483-21490
19. Aoki, H., Yokoyama, T., Fujiwara, K., Tari, A. M., Sawaya, R., Suki, D., Hess, K. R., Aldape, K. D., Kondo, S., Kumar, R., and Kondo, Y. (2007) Phosphorylated Pak1 level in the cytoplasm correlates with shorter survival time in patients with glioblastoma. *Clin. Cancer Res.* **13**, 6603-6609
20. Seo, M., Lee, S., Kim, J. H., Lee, W. H., Hu, G., Elledge, S. J., and Suk, K. (2014) RNAi-based functional selection identifies novel cell migration determinants dependent on PI3K and AKT pathways. *Nat. Commun.* **5**, 5217
21. Kim, J. H., Seo, Y., Jo, M., Jeon, H., Lee, W. H., Yachie, N., Zhong, Q., Vidal, M., Roth, F. P., and Suk, K. (2020) Yeast-Based Genetic Interaction Analysis of Human Kinome. *Cells* **9**, 1156
22. Youn, J. Y., Friesen, H., Nguyen Ba, A. N., Liang, W., Messier, V., Cox, M. J., Moses, A. M., and Andrews, B. (2017) Functional Analysis of Kinases and Transcription Factors in Saccharomyces cerevisiae Using an Integrated Overexpression Library. *G3 (Bethesda)* **7**, 911-921
23. Lee, K. T., So, Y. S., Yang, D. H., Jung, K. W., Choi, J., Lee, D. G., Kwon, H., Jang, J., Wang, L. L., Cha, S., Meyers, G. L., Jeong, E., Jin, J. H., Lee, Y., Hong, J., Bang, S., Ji, J. H., Park, G., Byun, H. J., Park, S. W., Park, Y. M., Adedoyin, G., Kim, T., Averette, A. F., Choi, J. S., Heitman, J., Cheong, E., Lee, Y. H., and Bahn, Y. S. (2016) Systematic functional analysis of kinases in the fungal pathogen Cryptococcus neoformans. *Nat Commun* **7**, 12766
24. Sharifpoor, S., van Dyk, D., Costanzo, M., Baryshnikova, A., Friesen, H., Douglas, A. C., Youn, J. Y., VanderSluis, B., Myers, C. L., Papp, B., Boone, C., and Andrews, B. J. (2012) Functional wiring of the yeast kinome revealed by global analysis of genetic network motifs. *Genome Res* **22**, 791-801
25. Botstein, D., and Fink, G. R. (2011) Yeast: an experimental organism for 21st Century biology. *Genetics* **189**, 695-704

26. Giaever, G., Shoemaker, D. D., Jones, T. W., Liang, H., Winzeler, E. A., Astromoff, A., and Davis, R. W. (1999) Genomic profiling of drug sensitivities via induced haploinsufficiency. *Nat Genet* **21**, 278-283
27. Smith, A. M., Durbic, T., Kittanakom, S., Giaever, G., and Nislow, C. (2012) Barcode sequencing for understanding drug-gene interactions. *Methods Mol Biol* **910**, 55-69
28. Smith, A. M., Heisler, L. E., Mellor, J., Kaper, F., Thompson, M. J., Chee, M., Roth, F. P., Giaever, G., and Nislow, C. (2009) Quantitative phenotyping via deep barcode sequencing. *Genome Res* **19**, 1836-1842
29. Smith, A. M., Heisler, L. E., St Onge, R. P., Farias-Hesson, E., Wallace, I. M., Bodeau, J., Harris, A. N., Perry, K. M., Giaever, G., Pourmand, N., and Nislow, C. (2010) Highly-multiplexed barcode sequencing: an efficient method for parallel analysis of pooled samples. *Nucleic Acids Res* **38**, e142
30. Jo, M., Chung, A. Y., Yachie, N., Seo, M., Jeon, H., Nam, Y., Seo, Y., Kim, E., Zhong, Q., Vidal, M., Park, H. C., Roth, F. P., and Suk, K. (2017) Yeast genetic interaction screen of human genes associated with amyotrophic lateral sclerosis: identification of MAP2K5 kinase as a potential drug target. *Genome Res* **27**, 1487-1500
31. Kim, J. H., Seo, Y., Jo, M., Jeon, H., Lee, W. H., Yachie, N., Zhong, Q., Vidal, M., Roth, F. P., and Suk, K. (2020) Yeast-Based Genetic Interaction Analysis of Human Kinome. *Cells* **9**
32. O'Brien, K. P., Remm, M., and Sonnhammer, E. L. (2005) Inparanoid: a comprehensive database of eukaryotic orthologs. *Nucleic Acids Res* **33**, D476-480
33. Kim, H., Oh, J. Y., Choi, S. L., Nam, Y. J., Jo, A., Kwon, A., Shin, E. Y., Kim, E. G., and Kim, H. K. (2016) Down-regulation of p21-activated serine/threonine kinase 1 is involved in loss of mesencephalic dopamine neurons. *Mol Brain* **9**, 45
34. Lun, X. K., Szklarczyk, D., Gabor, A., Dobberstein, N., Zanotelli, V. R. T., Saez-Rodriguez, J., von Mering, C., and Bodenmiller, B. (2019) Analysis of the Human Kinome and Phosphatome by Mass Cytometry Reveals Overexpression-Induced Effects on Cancer-Related Signaling. *Mol Cell* **74**, 1086-1102 e1085
35. Ishikawa, E., Kosako, H., Yasuda, T., Ohmuraya, M., Araki, K., Kurosaki, T., Saito, T., and Yamasaki, S. (2016) Protein kinase D regulates positive selection of CD4(+) thymocytes through phosphorylation of SHP-1. *Nat Commun* **7**, 12756
36. Camurdanoglu, B. Z., Hrovat, C., Durnberger, G., Madalinski, M., Mechtler, K., and Herbst, R. (2016) MuSK Kinase Activity is Modulated By A Serine Phosphorylation Site in The Kinase Loop. *Sci Rep* **6**, 33583
37. Koch, A., Maia, A., Janssen, A., and Medema, R. H. (2016) Molecular basis underlying resistance to Mps1/TTK inhibitors. *Oncogene* **35**, 2518-2528
38. Wang, Y. D., Su, Y. J., Li, J. Y., Yao, X. C., and Liang, G. J. (2015) Rapamycin, a mTOR inhibitor, induced growth inhibition in retinoblastoma Y79 cell via down-regulation of Bmi-1. *Int. J. Clin. Exp. Pathol.* **8**, 5182-5188
39. Jiang, P., Mukthavaram, R., Chao, Y., Bharati, I. S., Fogal, V., Pastorino, S., Cong, X., Nomura, N., Gallagher, M., Abbasi, T., Vali, S., Pingle, S. C., Makale, M., and Kesari, S. (2014) Novel anti-glioblastoma agents and therapeutic combinations identified from a collection of FDA approved drugs. *J. Transl. Med.* **12**, 13
40. Garcia-Saez, I., DeBonis, S., Lopez, R., Trucco, F., Rousseau, B., Thuery, P., and Kozielski, F. (2007) Structure of human Eg5 in complex with a new monastrol-based inhibitor bound in the R configuration. *J. Biol. Chem.* **282**, 9740-9747
41. Wiese, E. K., and Hitosugi, T. (2018) Tyrosine Kinase Signaling in Cancer Metabolism: PKM2 Paradox in the Warburg Effect. *Front. Cell Dev. Biol.* **6**, 79

42. Lu, Z., and Hunter, T. (2018) Metabolic Kinases Moonlighting as Protein Kinases. *Trends Biochem. Sci.* **43**, 301-310
43. Dayton, T. L., Jacks, T., and Vander Heiden, M. G. (2016) PKM2, cancer metabolism, and the road ahead. *EMBO Rep.* **17**, 1721-1730
44. Johnston, S. T., Shah, E. T., Chopin, L. K., Sean McElwain, D. L., and Simpson, M. J. (2015) Estimating cell diffusivity and cell proliferation rate by interpreting IncuCyte ZOOM assay data using the Fisher-Kolmogorov model. *BMC Syst Biol* **9**, 38
45. Aslan, J. E., Baker, S. M., Loren, C. P., Haley, K. M., Itakura, A., Pang, J., Greenberg, D. L., David, L. L., Manser, E., Chernoff, J., and McCarty, O. J. (2013) The PAK system links Rho GTPase signaling to thrombin-mediated platelet activation. *Am J Physiol Cell Physiol* **305**, C519-528
46. Tang, Y., Zhou, H., Chen, A., Pittman, R. N., and Field, J. (2000) The Akt proto-oncogene links Ras to Pak and cell survival signals. *J. Biol. Chem.* **275**, 9106-9109
47. Thillai, K., Lam, H., Sarker, D., and Wells, C. M. (2017) Deciphering the link between PI3K and PAK: An opportunity to target key pathways in pancreatic cancer? *Oncotarget* **8**, 14173-14191
48. Xue, G., and Hemmings, B. A. (2013) PKB/Akt-dependent regulation of cell motility. *J. Natl. Cancer Inst.* **105**, 393-404
49. Higuchi, M., Onishi, K., Kikuchi, C., and Gotoh, Y. (2008) Scaffolding function of PAK in the PDK1-Akt pathway. *Nat. Cell Biol.* **10**, 1356-1364
50. Taga, M., Hirooka, E., and Ouchi, T. (2009) Essential roles of mTOR/Akt pathway in Aurora-A cell transformation. *Int. J. Biol. Sci.* **5**, 444-450
51. Sarbassov, D. D., Guertin, D. A., Ali, S. M., and Sabatini, D. M. (2005) Phosphorylation and regulation of Akt/PKB by the rictor-mTOR complex. *Science* **307**, 1098-1101
52. Kim, S. R., Kareva, T., Yarygina, O., Kholodilov, N., and Burke, R. E. (2012) AAV transduction of dopamine neurons with constitutively active Rheb protects from neurodegeneration and mediates axon regrowth. *Mol Ther* **20**, 275-286
53. Ries, V., Henchcliffe, C., Kareva, T., Rzhetskaya, M., Bland, R., During, M. J., Kholodilov, N., and Burke, R. E. (2006) Oncoprotein Akt/PKB induces trophic effects in murine models of Parkinson's disease. *Proc Natl Acad Sci U S A* **103**, 18757-18762
54. Alimova, I., Ng, J., Harris, P., Birks, D., Donson, A., Taylor, M. D., Foreman, N. K., Venkataraman, S., and Vibhakar, R. (2016) MPS1 kinase as a potential therapeutic target in medulloblastoma. *Oncol. Rep.* **36**, 2633-2640
55. Wei, J. H., Chou, Y. F., Ou, Y. H., Yeh, Y. H., Tyan, S. W., Sun, T. P., Shen, C. Y., and Shieh, S. Y. (2005) TTK/hMps1 participates in the regulation of DNA damage checkpoint response by phosphorylating CHK2 on threonine 68. *J. Biol. Chem.* **280**, 7748-7757
56. Be Tu, P. T., Nguyen, B. C., Tawata, S., Yun, C. Y., Kim, E. G., and Maruta, H. (2017) The serum/PDGF-dependent "melanogenic" role of the minute level of the oncogenic kinase PAK1 in melanoma cells proven by the highly sensitive kinase assay. *Drug Discov. Ther.* **10**, 314-322
57. Rahman, M. H., Jha, M. K., Kim, J. H., Nam, Y., Lee, M. G., Go, Y., Harris, R. A., Park, D. H., Kook, H., Lee, I. K., and Suk, K. (2016) Pyruvate Dehydrogenase Kinase-mediated Glycolytic Metabolic Shift in the Dorsal Root Ganglion Drives Painful Diabetic Neuropathy. *J. Biol. Chem.* **291**, 6011-6025
58. Shin, K. S., Shin, E. Y., Lee, C. S., Quan, S. H., Woo, K. N., Soung, N. K., Kwak, S. J., Kim, S. R., and Kim, E. G. (2002) Basic fibroblast growth factor-induced translocation of p21-

activated kinase to the membrane is independent of phospholipase C-gamma1 in the differentiation of PC12 cells. *Exp. Mol. Med.* **34**, 172-176
59. Alberti, S., Gitler, A. D., and Lindquist, S. (2007) A suite of Gateway cloning vectors for high-throughput genetic analysis in Saccharomyces cerevisiae. *Yeast* **24**, 913-919
60. Gietz, R. D., and Schiestl, R. H. (2007) High-efficiency yeast transformation using the LiAc/SS carrier DNA/PEG method. *Nat Protoc* **2**, 31-34
61. Liang, C. C., Park, A. Y., and Guan, J. L. (2007) In vitro scratch assay: a convenient and inexpensive method for analysis of cell migration in vitro. *Nat. Protoc.* **2**, 329-333
62. Aaberg-Jessen, C., Norregaard, A., Christensen, K., Pedersen, C. B., Andersen, C., and Kristensen, B. W. (2013) Invasion of primary glioma- and cell line-derived spheroids implanted into corticostriatal slice cultures. *Int. J. Clin. Exp. Pathol.* **6**, 546-560
63. Norregaard, A., Jensen, S. S., Kolenda, J., Aaberg-Jessen, C., Christensen, K. G., Jensen, P. H., Schroder, H. D., and Kristensen, B. W. (2012) Effects of chemotherapeutics on organotypic corticostriatal slice cultures identified by a panel of fluorescent and immunohistochemical markers. *Neurotox. Res.* **22**, 43-58
64. Stoppini, L., Buchs, P. A., and Muller, D. (1991) A simple method for organotypic cultures of nervous tissue. *J. Neurosci. Methods* **37**, 173-182
65. Eisemann, T., Costa, B., Strelau, J., Mittelbronn, M., Angel, P., and Peterziel, H. (2018) An advanced glioma cell invasion assay based on organotypic brain slice cultures. *BMC Cancer* **18**, 103
66. Depner, C., Zum Buttel, H., Bogurcu, N., Cuesta, A. M., Aburto, M. R., Seidel, S., Finkelmeier, F., Foss, F., Hofmann, J., Kaulich, K., Barbus, S., Segarra, M., Reifenberger, G., Garvalov, B. K., Acker, T., and Acker-Palmer, A. (2016) EphrinB2 repression through ZEB2 mediates tumour invasion and anti-angiogenic resistance. *Nat. Commun.* **7**, 12329
67. Yadav, V. N., Zamler, D., Baker, G. J., Kadiyala, P., Erdreich-Epstein, A., DeCarvalho, A. C., Mikkelsen, T., Castro, M. G., and Lowenstein, P. R. (2016) CXCR4 increases in-vivo glioma perivascular invasion, and reduces radiation induced apoptosis: A genetic knockdown study. *Oncotarget* **7**, 83701-83719
68. Candolfi, M., Curtin, J. F., Nichols, W. S., Muhammad, A. G., King, G. D., Pluhar, G. E., McNiel, E. A., Ohlfest, J. R., Freese, A. B., Moore, P. F., Lerner, J., Lowenstein, P. R., and Castro, M. G. (2007) Intracranial glioblastoma models in preclinical neuro-oncology: neuropathological characterization and tumor progression. *J. Neurooncol.* **85**, 133-148
69. Lampson, L. A., Lampson, M. A., and Dunne, A. D. (1993) Exploiting the lacZ reporter gene for quantitative analysis of disseminated tumor growth within the brain: use of the lacZ gene product as a tumor antigen, for evaluation of antigenic modulation, and to facilitate image analysis of tumor growth in situ. *Cancer Res.* **53**, 176-182
70. Cortes-Santiago, N., Hossain, M. B., Gabrusiewicz, K., Fan, X., Gumin, J., Marini, F. C., Alonso, M. M., Lang, F., Yung, W. K., Fueyo, J., and Gomez-Manzano, C. (2016) Soluble Tie2 overrides the heightened invasion induced by anti-angiogenesis therapies in gliomas. *Oncotarget* **7**, 16146-16157
71. Feng, H., Hu, B., Vuori, K., Sarkaria, J. N., Furnari, F. B., Cavenee, W. K., and Cheng, S. Y. (2014) EGFRvIII stimulates glioma growth and invasion through PKA-dependent serine phosphorylation of Dock180. *Oncogene* **33**, 2504-2512
72. Feng, H., Hu, B., Liu, K. W., Li, Y., Lu, X., Cheng, T., Yiin, J. J., Lu, S., Keezer, S., Fenton, T., Furnari, F. B., Hamilton, R. L., Vuori, K., Sarkaria, J. N., Nagane, M., Nishikawa, R., Cavenee, W. K., and Cheng, S. Y. (2011) Activation of Rac1 by Src-dependent

phosphorylation of Dock180(Y1811) mediates PDGFRalpha-stimulated glioma tumorigenesis in mice and humans. *J. Clin. Invest.* **121**, 4670-4684
73. Charan, J., and Kantharia, N. D. (2013) How to calculate sample size in animal studies? *J Pharmacol Pharmacother* **4**, 303-306

Tables

Table 1. List of PAK1 genetic interactions expressed in glioma cells.

No.	Yeast gene names		UniProt ID	Description	Human orthologs
1	YMR246W	FAA4	P47912	Long-chain-fatty-acid--CoA ligase 4, EC 6.2.1.3 (fatty acid activator 4) (long-chain acyl-CoA synthetase 4)	ACSL4
2	YHR028C	DAP2	P18962	Dipeptidyl aminopeptidase B, DPAP B, EC 3.4.14.- (YSCV)	DPP4
3	YCL011C	GBP2	P25555	Single-strand telomeric DNA-binding protein GBP2, G-strand-binding protein 2 (RAP1 localization factor 6)	ELAVL1
4	YBL003C	HTA2	P04912	Histone H2A.2	H2AFX
5	YBR010W	HHT1	P61830	Histone H3	H3F3A
6	YAL005C	SSA1	P10591	Heat shock protein SSA1 (heat shock protein YG100)	HSPA8
7	YEL009C	GCN4	P03069	General control protein GCN4 (amino acid biosynthesis regulatory protein)	JUNB
8	YBL063W	KIP1	P28742	Kinesin-like protein KIP1 (chromosome instability protein 9)	KIF11
9	YER007C-A	TMA20	P89886	Translation machinery-associated protein 20	MCTS1
10	YBL091C	MAP2	P38174	Methionine aminopeptidase 2, MAP 2, MetAP 2, EC 3.4.11.18 (peptidase M)	METAP2
11	YJR066W	TOR1	P35169	Serine/threonine-protein kinase TOR1, EC 2.7.11.1 (dominant rapamycin resistance protein 1) (phosphatidylinositol kinase homolog TOR1) (target of rapamycin kinase 1)	mTOR
12	YPL006W	NCR1	Q12200	NPC intracellular cholesterol transporter 1-related protein 1 (Niemann-Pick type C-related protein 1)	NPC1

13	YBL024W	NCL1	P38205	Multisite-specific tRNA:(cytosine-C(5))-methyltransferase, EC 2.1.1.202 (multisite-specific tRNA:m5C-methyltransferase) (tRNA (cytosine-5-)-methyltransferase NCL1) (tRNA methyltransferase 4)	NSUN2
14	YOR347C	PYK2	P52489	Pyruvate kinase 2, PK 2, EC 2.7.1.40	PKM1, PKM2
15	YJR100C	AIM25	P47140	Altered inheritance rate of mitochondria protein 25	PLSCR1
16	YJL134W	LCB3	P47013	Dihydrosphingosine 1-phosphate phosphatase LCB3, EC 3.1.3.- (long-chain base protein 3) (sphingolipid resistance protein 2)	SGPP1
17	YHR114W	BZZ1	P38822	Protein BZZ1 (LAS17-binding protein 7)	TRIP10
18	YCR008W	SAT4	P25333	Serine/threonine-protein kinase HAL4/SAT4, EC 2.7.11.1 (halotolerance protein 4)	TTK
19	YER177W	BMH1	P29311	Protein BMH1	YWHAE

Table 2. Evaluation of candidate PAK1 human genetic interactions with respect to cell migration using siRNAs.

Serial No.	Gene name	siRNA No.	Migration assay [a]	
			GL26-PAK1-1	GL26-PAK1-2
1	ACSL4	5	−	−
2	DPP4	1	+	+
3	ELAVL1	5	−	−
4	H2AFX	1	−	−
5	H3F3A	1	−	−
6	HSPA8	1	−	−
7	JUNB	2	−	−
8	KIF11	5	+	+
9	MCTS1	1	−	−
10	METAP2	1	−	−
11	mTOR	1	+	+
12	NPC1	1	−	−
13	NSUN2	3	−	−
14	PKM1	4	−	−
15	PKM2	6	+	+
16	PLSCR1	4	−	−
17	SGPP1	1	+	+
18	TRIP10	5	−	−
19	TTK	1	+	+
20	YWHAE	5	+	+

[a] Genetic interaction with *P*-value tested by wound healing assay in two independent clones of PAK1 stable transfectants (GL26-PAK1-1, GL26-PAK1-2) (+, $P < 0.05$; −, not significant).

Table 3. Evaluation of candidate PAK1 genetic interactions with respect to cell migration using pharmacological inhibitors.

Serial No.	Gene name	Inhibitor name	Migration assay [a]	
			GL26-PAK1-1	GL26-PAK1-2
1	DPP4	Vildagliptin	+	+
2	KIF11	Monastrol	+	+
3	METAP2	Fumagillin	−	−
4	mTOR	Rapamycin	+	+
5	PKM2	P-M2tide	−	−
6	TTK	MPS1-IN-1	+	+

[a] Genetic interaction with *P*-value tested by wound healing assay in two independent clones of PAK1 stable transfectants (GL26-PAK1-1, GL26-PAK1-2) (+, $P < 0.05$; −, not significant).

Table 4. Evaluation of candidate PAK1 genetic interactions with respect to drug resistance using siRNAs.

Serial No.	Gene name	siRNA No.	LDH assay [a]		MTT assay [b]	
			GL26-PAK1-1	GL26-PAK1-2	GL26-PAK1-1	GL26-PAK1-2
1	ACSL4	5	−	−	−	−
2	DPP4	1	+	+	+	++
3	ELAVL1	5	−	−	−	−
4	H2AFX	1	−	−	−	−
5	H3F3A	1	−	−	−	−
6	HSPA8	1	−	−	−	−
7	JUNB	2	−	−	−	−
8	KIF11	5	−	−	−	−
9	MCTS1	1	−	−	−	−
10	METAP2	1	−	−	−	−
11	mTOR	1	+	++	+	+
12	NPC1	1	−	−	−	−
13	NSUN2	3	−	−	−	−
14	PKM1	4	−	−	−	−
15	PKM2	6	−	−	−	−
16	PLSCR1	4	−	−	−	−
17	SGPP1	1	+	++	+	++
18	TRIP10	5	−	−	−	−
19	TTK	1	++	+	++	+
20	YWHAE	5	++	+	+	+

[a] Genetic interaction with *P*-value tested by LDH assay in two independent clones of PAK1 stable transfectants (GL26-PAK1-1, GL26-PAK1-2) (+, $P < 0.05$; ++, $P < 0.01$; −, not significant).

[b] Genetic interaction with *P*-value tested by MTT assay in two independent clones of PAK1 stable transfectants (GL26-PAK1-1, GL26-PAK1-2) (+, $P < 0.05$; ++, $P < 0.01$; −, not significant).

Table 5. Evaluation of PAK1 genetic interactions with respect to cell proliferation using pharmacological inhibitors.

Serial No.	Gene name	Inhibitor name	Proliferation assay [a]	
			GL26-PAK1-1	GL26-PAK1-2
1	DPP4	Vildagliptin	+	++
2	KIF11	Monastrol	−	−
3	METAP2	Fumagillin	++	+
4	mTOR	Rapamycin	+	+
5	PKM2	P-M2tide	++	+
6	TTK	MPS1-IN-1	+	++

[a] Genetic interaction with *P*-value tested by cell proliferation assay in two independent clones of PAK1 stable transfectants (GL26-PAK1-1, GL26-PAK1-2) (+, $P < 0.05$; ++, $P < 0.01$; −, not significant).

Figures

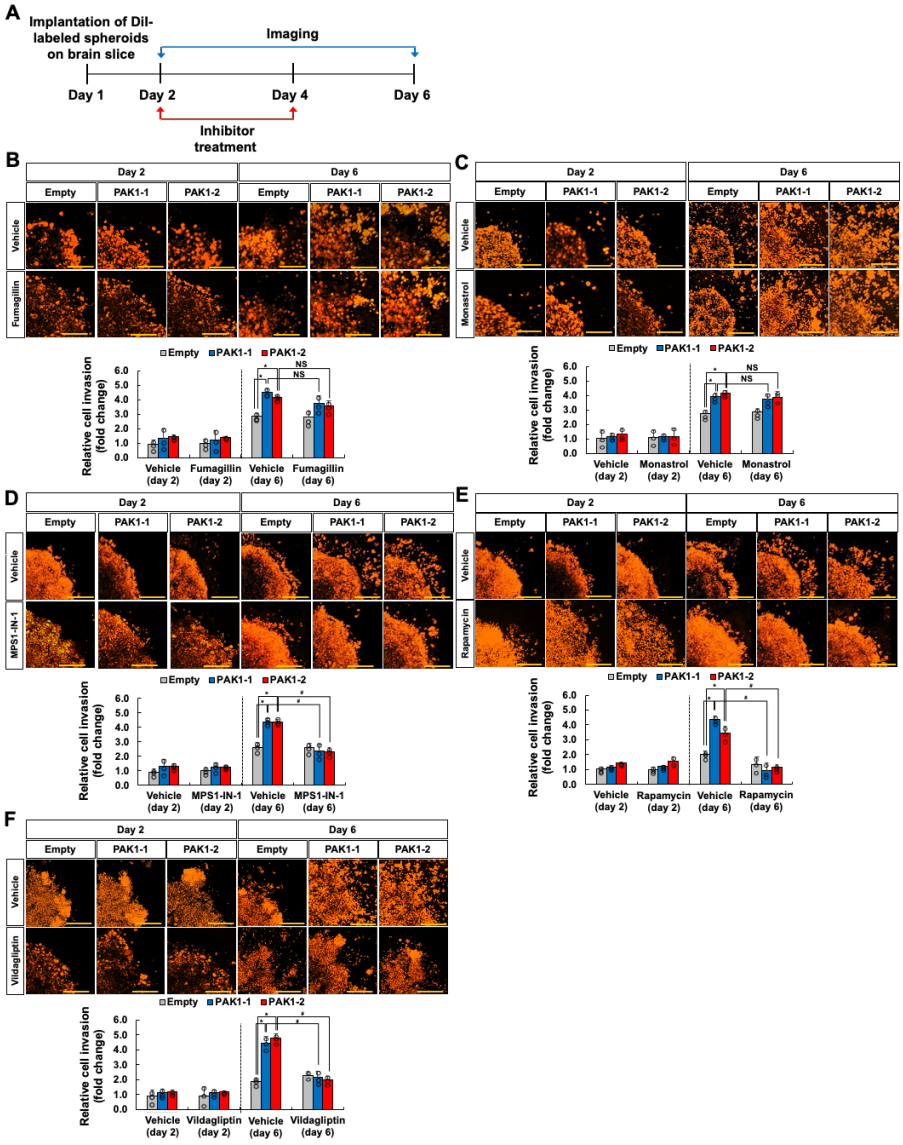

Figure 1. Evaluation of PAK1 genetic interactions in organotypic brain slices. (**A**) Experimental timeline. DiI-labeled spheroids were implanted onto brain slice cultures on day 1. Confocal imaging and inhibitor treatment were performed at the given time points. *B–F*) GL26 glioma spheroids stably expressing empty vector or PAK1 (GL26-PAK1-1, GL26-PAK1-2) were implanted onto the slice cultures followed by treatment with vehicle or pharmacological inhibitors of potential PAK1 interaction partners: (**B**) fumagillin, 1 nM; (**C**) monastrol, 1 µM; (**D**) MPS1-IN-1, 100 nM; (**E**) rapamycin, 100 nM; (**F**) vildagliptin, 250 nM. The z-stack images were superimposed into a single image representing the entire spheroid. Invasive cell density was quantified as shown in the graphs. *Scale bar*, 200 µm. $*P < 0.05$ (Student's *t*-test comparing empty versus PAK1 groups, n=3); $^{\#}P < 0.05$ (Student's *t*-test comparing vehicle versus inhibitor groups, n=3); NS, not significant. All error bars represent s.d.

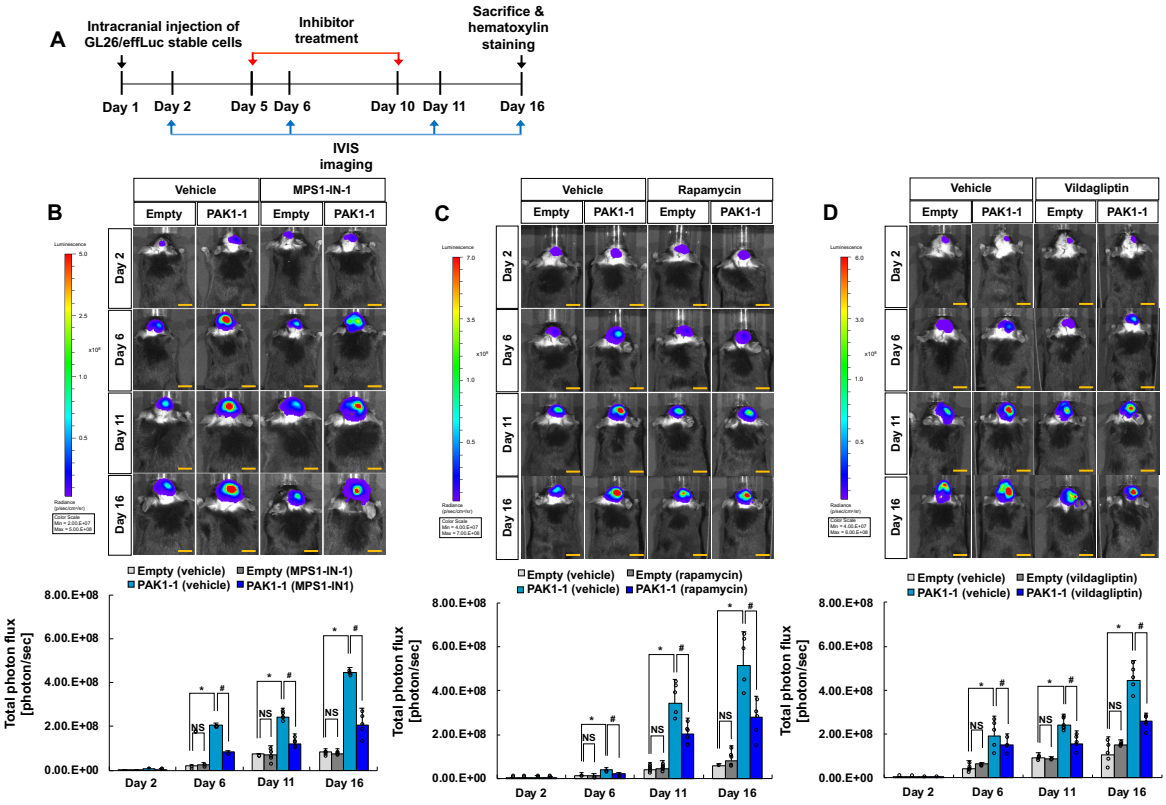

Figure 2. Evaluation of PAK1 genetic interactions in an orthotopic model of glioma. (**A**) Experimental timeline. C57BL/6 mice were injected with 9×10^5 empty- or PAK1-expressing GL26-effLuc cells in the striatum. Glioma-implanted mice were injected with inhibitors (MPS1-IN-1, rapamycin, or vildagliptin) or vehicle, and IVIS images were obtained at the indicated time points to assess glioma growth. *B–D*) IVIS images were collected on days 2, 6, 11, and 16, and glioma growth in the presence of vehicle or inhibitors was quantified in the graphs: (**B**) MPS1-IN-1, 100 nM, 5 µl; (**C**) rapamycin, 100 nM, 5 µl; (**D**) vildagliptin, 250 nM, 5 µl. Photon intensity of the images is directly related to tumor size. *Scale bar*, 5 mm. $^*P < 0.05$ (Student's *t*-test comparing empty versus PAK1-1 group, n=5); $^{\#}P < 0.05$ (Student's *t*-test comparing vehicle versus inhibitor groups, n=5); NS, not significant. All error bars represent s.d.

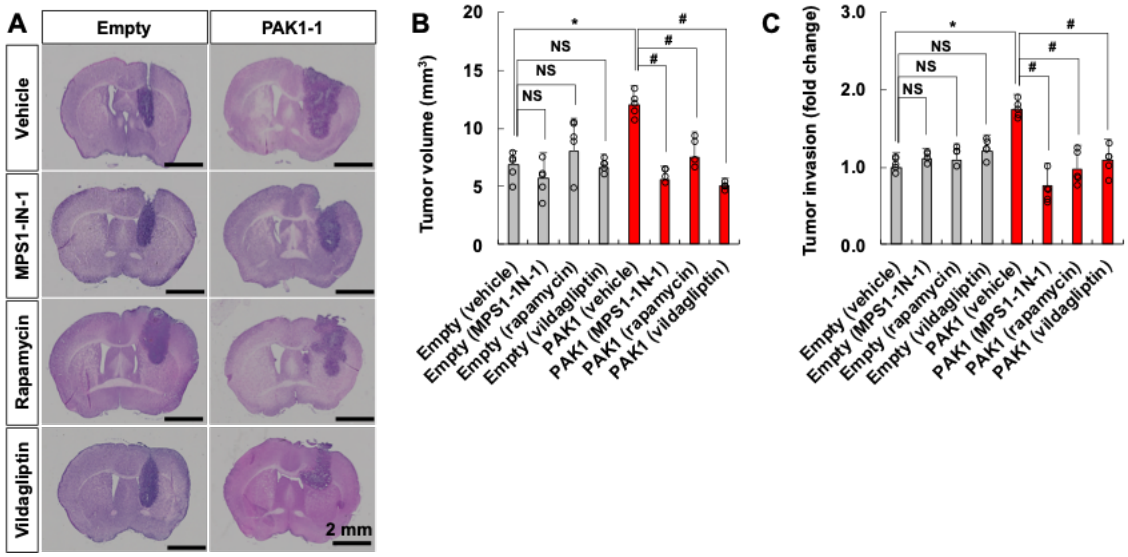

Figure 3. Assessment of tumor volume and invasiveness in an orthotopic model of glioma. After IVIS imaging (as in Figure 2), mice (n=5) from each group (empty vector- or PAK1-transfected GL26 glioma cells implanted; vehicle or inhibitors injected) were euthanized to obtain brain tissues, and the tumor volume (**A**, **B**) and invasiveness (**C**) were evaluated. (**A**) Representative hematoxylin-stained images from serial sections confirm viable regions of tumor. (**B**) Tumor volume was calculated by quantitative digital image analysis of the serial sections containing tumor. (**C**) Overall tumor invasion was quantified by particle analysis of threshold images prepared from tumor-bearing sections of engrafted animals. Tumor invasion in each group of animals was assessed by counting the number of tumor particles invading the brain parenchyma per tumor rim length. *Scale bar*, 2 mm. *P < 0.05 (Student's t-test, n=5); $^{\#}P$ < 0.05 (Student's t-test, n=5); NS, not significant. All error bars represent s.d.

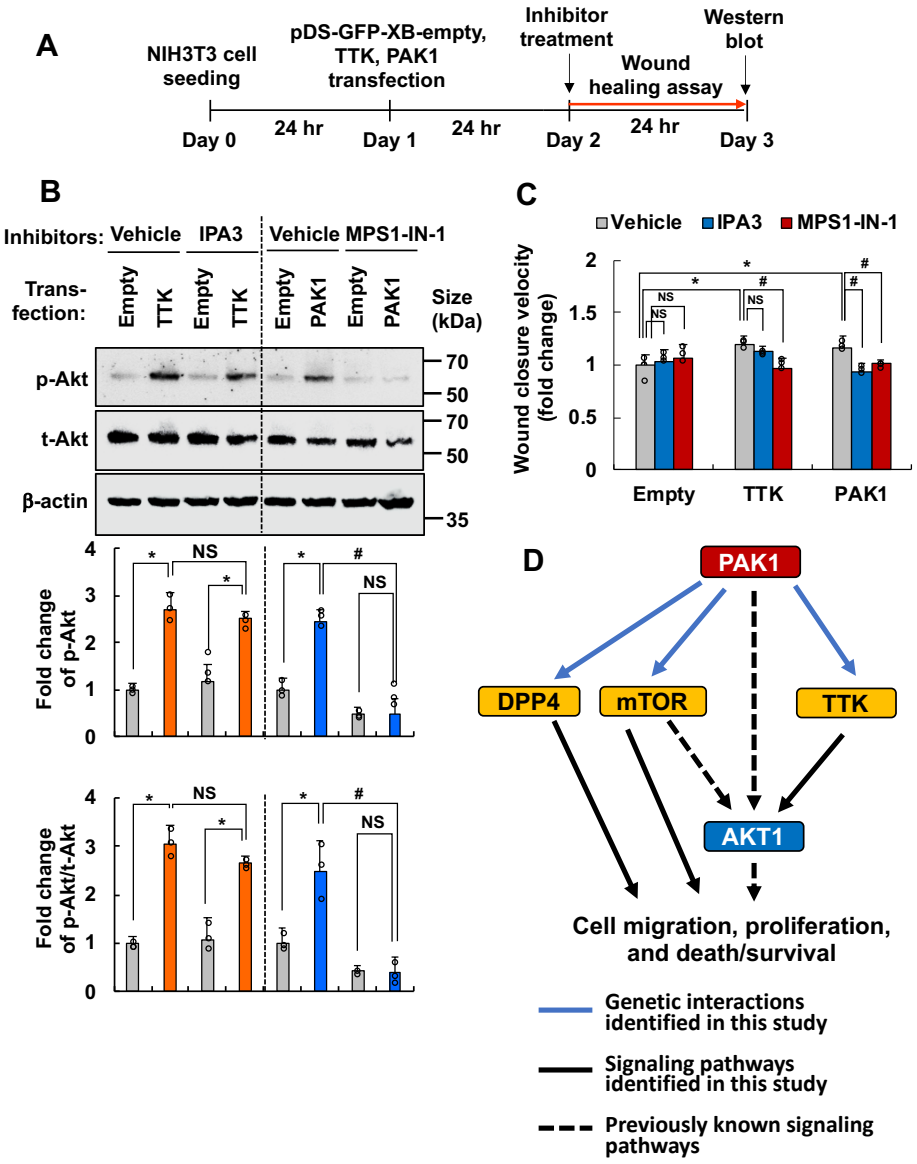

Figure 4. Role of AKT1 in the genetic interaction between PAK1 and TTK. (**A**) Experimental timeline. NIH3T3 cells were transiently transfected with empty vector, *PAK1*, or *TTK* cDNAs; treated with inhibitors (TTK inhibitor, MPS1-IN-1; PAK1 inhibitor, IPA3); and signaling pathway or cell migration was analyzed by western blotting or wound healing assay, respectively. (**B**) Phospho-AKT (p-AKT), total AKT (t-AKT), or β-actin protein levels were measured by western blotting. Quantification of the band intensities is presented in the adjacent graphs. $*P < 0.05$ (Student's *t*-test, $n=3$); $^{\#}P < 0.05$ (Student's *t*-test, $n=3$). (**C**) Quantification of cell migration based on the wound healing assays. $*P < 0.05$ (Student's *t*-test comparing empty- versus TTK- or PAK1-transfected group, $n=5$); $^{\#}P < 0.05$ (Student's *t*-test, $n=5$). All error bars represent s.d. (**D**) Schematic representation of the PAK1, TTK, and AKT pathways. The PAK1-TTK-AKT1 axis appears to play an important role in glioma migration/invasion, drug resistance, and proliferation. PAK1-mTOR or PAK1-DPP4 may play a similar role through either AKT1-dependent or -independent pathways.

Interrogation of kinase genetic interactions provides a global view of PAK1-mediated signal transduction pathways

Jae-Hong Kim, Yeojin Seo, Myungjin Jo, Hyejin Jeon, Young-Seop Kim, Eun-Jung Kim, Donggun Seo, Won-Ha Lee, Sang Ryong Kim, Nozomu Yachie, Quan Zhong, Marc Vidal, Frederick P. Roth and Kyoungho Suk

J. Biol. Chem. published online October 15, 2020

Access the most updated version of this article at doi: 10.1074/jbc.RA120.014831